The anti-HIV drug tipranavir induces gastric cancer stem cell apoptosis and exerts anticancer activity via the PRSS23–IL24 pathway

Jixian Xiong
Shenzhen University Health Science Center
Yuting Li
Shenzhen University Health Science Center
Xiangyu Tan
Shenzhen University Health Science Center
Tie Chen
Shenzhen University Health Science Center
Baohua Liu
Shenzhen University Health Science Center
Li Fu (gracelfu@szu.edu.cn)
Shenzhen University Health Science Center

Research Article

Keywords: Tipranavir, Gastric cancer stem cell, PRSS23, MKK3, p38 MAPK, IL24

Posted Date: May 18th, 2022

DOI: https://doi.org/10.21203/rs.3.rs-1660593/v1

Abstract

Gastric cancer stem cells (GCSCs) contribute substantially to the refractory features of gastric cancer (GC) and are responsible for metastasis, relapse and drug resistance. However, strategies aimed at eliminating GCSCs to improve the clinical outcome of GC patients remain a challenge. Here, we report that tipranavir, a clinically used anti-HIV drug, effectively killed both GCSC and GC cell lines, and inhibited tumor growth in GCSC-derived xenograft models without apparent toxicity. Mechanistic analyses demonstrated that tipranavir induced GCSC cell apoptosis by targeting the novel serine protease PRSS23, releasing MKK3 from the PRSS23/MKK3 complex to activate p38 MAPK, and thereby activating the interleukin (IL) 24-mediated Bax/Bak mitochondrial apoptotic pathway. Tipranavir also killed other types of cancer cell lines and drug-resistant cell lines. Our findings indicate that by targeting both GCSC and GC cells, tipranavir is a promising anti-cancer drug, and the clinical development of tipranavir or other drugs specifically targeting the PRSS23/MKK3/p38MAPK–IL24 mitochondrial apoptotic pathway may offer an effective approach to combat gastric and other cancers.

Background:

Gastric cancer (GC) is the fifth most commonly diagnosed cancer and the third leading cause of cancer-related death globally [1]. The highest incidence and mortality rates of GC occur in East Asian countries, accounting for ~ 60% of the total new cases and deaths worldwide [2]. In China, GC is the third leading cause of cancer incidence and mortality, with an estimated 478,508 new cases and 373,789 deaths in 2020 [3]. Most patients with GC are diagnosed at an advanced stage [4]. Thus, chemotherapy is the current preferred treatment in patients with primarily unresectable, advanced-stage GC [5]. Fluoropyrimidine- and platinum-based chemotherapy regimens, such as 5-fluorouracil (5-FU) in combination with cisplatin, are the most commonly used first-line treatments for advanced GC patients [6–8]. However, the prognosis of advanced GC patients remains poor, and the five-year overall survival rate is < 20% (with a median overall survival time of less than 12 months) due to recurrence and metastasis [9–11].

Cancer stem cells (CSCs) are a subpopulation of stem cell-like cancer cells that are responsible for all aspects of cancer pathogenesis including initiation, development, drug resistance, metastasis and cancer recurrence [12–14]. Traditional chemo- and radiotherapies kill most tumor cells but leave rare CSCs. These residual cells then regenerate the tumor or spread to form new tumors in other organs, and thus lead to tumor relapse, metastasis and treatment failure. Targeting CSCs can lead to tumor regression, and combining CSC-targeted therapy with conventional chemotherapy could eradicate the tumor [15–16]. Therefore, the development of CSC-targeting drugs for cancer research and clinical application is critical and urgent.

Gastric cancer stem cells (GCSCs) were first identified from human gastric cancer cell lines [17]. We previously identified and purified GCSCs from human gastric adenocarcinoma (GAC) tumor tissue, and showed that these cells can be expanded in vitro and form tumors in mice [18]. GCSC-targeting therapies

are currently being investigated in lab studies and clinical trials, including chemotherapeutic and biological agents that target GCSC surface markers, signaling pathways, and the CSC microenvironment [19, 20]. However, only a few agents that target these molecules have been identified. Further clinical studies are needed to prove the clinical significance of these agents [19, 21], and there are no therapies that target GCSCs therapies approved for clinical use. To date, no agents can efficiently eliminate both GCSCs and GC cells.

Multiple studies indicate that human immunodeficiency virus (HIV) protease inhibitors (PIs) such as nelfinavir have anti-cancer effects [22–25], suggesting they could be suitable candidates for drug repurposing for cancer.

In the present study, we found that the anti-HIV drug tipranavir killed GCSC cells by activating the PRSS23/MKK3/p38-IL24-Bax/Bak mitochondrial apoptotic pathway, and inhibited the growth of GCSC-derived tumor xenografts in nude mice with little toxicity on non-cancerous cells. Moreover, tipranavir killed GC cells as well as other types of tumor cells. Collectively, our results show that by targeting both GCSC and GC cells, tipranavir could be a promising and effective treatment for gastric cancer.

Methods:

Reagents and antibodies. Atazanavir, darunavir, fosamprenavir, tipranavir, 5-FU and cisplatin were purchased from MedChemExpress. Poloxamer 188 (F68) was obtained from Shenyang Jiqi Pharmaceutical Company. Antibodies against Bcl-2 (#4223), Bcl-xL (#2764), Bax (#5023), Bak (#12105), cleaved caspase-9 (#7237), cleaved caspase-7 (#8438), cleaved caspase-3 (#9661), cleaved PARP (#5625), p38 MAPK (#8690), phosphorylated p38 MAPK (#4511), phosphorylated MKK3/MKK6 (#12280), GAPDH (#5174), and VDAC (#4866) were purchased from Cell Signaling Technology. The antibody against PRSS23 (#ab201182) was from Abcam. The antibody against CEBPβ (#sc-7962) was from Santa Cruz Biotechnology. The antibody against IL24 (#26772-1-AP), MKK3 (#13898-1-AP), MKK4 (#17340-1-AP), MKK6 (#12745-1-AP) was from Proteintech. The antibody against cytochrome c (#556433) was from BD Biosciences. The secondary antibodies anti-rabbit (#7074) and anti-mouse (#7076) were obtained from Cell Signaling Technology.

Cell culture. Freshly isolated, primary tumor-derived GCSC cell lines (GCSC1 and GCSC2) were obtained from Dr Xianming Mo (Sichuan University), and were grown and maintained as previously described [18]. AGS, HGC-27, MGC-803, BGC-823, GES-1, PC9, PC3, HCT116, MDA-MB-231 and Huh7 cells were obtained from Cobioer Biosciences. KYSE180 and KYSE520 cells were obtained from DSMZ, the German Resource Centre for Biological Material. PC3/Tax cells were provided by Dr Xiangwei Wang (Shenzhen University General Hospital) [53]. AGS, HGC-27, MGC-803, BGC-823, GES-1, PC9 and HCT116 cells were cultured in RPMI (Gibco) with 10% FBS (Gibco) and penicillin/streptomycin (Gibco). KYSE180, KYSE520, MDA-MB-231 and Huh7 cells were cultured in DMEM (Gibco) with 10% FBS and penicillin/streptomycin. PC3 cells were cultured in DMEM/F12 (Gibco) with 10% FBS and penicillin/streptomycin. PC3/Tax cells were

cultured in DMEM/F12 with 10% FBS, paclitaxel (10 μM, Selleckchem), and penicillin/streptomycin. All cell lines were mycoplasma negative.

RNA extraction and qRT-PCR analysis. Total RNA was extracted using TRIzol reagent (Life Technologies) according to the manufacturer's instructions. RNA was reverse-transcribed into cDNA using PrimeScript RT Master Mix (Takara Biotechnology) and qPCR was conducted using TB Green Premix Ex Taq (Takara Biotechnology) on a CFX96 real-time PCR detection system (Bio-Rad Laboratories). GAPDH was used as an internal control and the 2-ΔΔCT method was used to quantify the relative mRNA expression of each gene. The sequences of primers used in this study were as follows:

PRSS23-F: 5'-CAGTGTCATAAGGGAACTCCAC-3'

PRSS23-R: 5'-CCTGAGTCTCGGTGTTGGG-3'

CEBPβ-F: 5'-AGAAGACCGTGGACAAGCAC-3'

CEBPβ-R: 5'-GCTTGAACAAGTTCCGCAGG-3'

IL24-F: 5'-TTGCCTGGGTTTTACCCTGC-3'

IL24-R: 5'-AAGGCTTCCCACAGTTTCTGG-3'

GAPDH-F: 5'-CGAGATCCCTCCAAAATCAA-3'

GAPDH-R: 5'-ATCCACAGTCTTCTGGGTGG-3'

Western blot analysis. Cultured cells or in vivo tumor tissues were lysed in RIPA buffer supplemented with protease and phosphatase inhibitors. Protein concentration was determined by the BCA assay (Thermo Fischer Scientific). Equal amounts of protein were separated by SDS–PAGE, transferred to PVDF membranes (Bio-Rad) and probed overnight at 4°C with the following primary antibodies: anti-Bax (1:2000), anti-Bak (1:2000), anti-Bcl-2 (1:2000), anti-Bcl-xL (1:2000), anti-cleaved caspase-9 (1:1000), anti-cleaved caspase-7 (1:1000), anti-cleaved caspase-3 (1:1000), anti-cleaved PARP (1:2000), anti-GAPDH (1:5000), anti-MKK3 (1:2000), anti-MKK4 (1:2000), anti-MKK6 (1:2000), anti-phospho MKK3/MKK6 (1:2000), anti-p38 MAPK (1:2000), anti-phospho p38 MAPK (1:2000), anti-VDAC (1:2000), anti-cytochrome c (1:2000), anti-PRSS23 (1:1000), anti-CEBPβ (1:500), anti-IL-24 (1:1000). The secondary antibodies used were anti-rabbit-HRP (1:5000) or anti-mouse-HRP (1:5000). Blots were developed using Immobilon western chemiluminescent HRP substrate (Millipore) or SuperSignal west chemiluminescent substrate (Thermo Fisher Scientific), and imaged using a ChemiDoc MP imaging system (BioRad). The band intensity was quantified using Image Lab software (Bio-Rad).

Cell viability assay. Cell viability was analyzed using a cell counting kit-8 (CCK-8) (Dojindo Kumamoto) following the manufacturer's instructions. Exponentially growing cells were seeded into 96-well culture

plates (5×10^4 cells/ml) in 100 ul of medium for 24 h. Cells were treated for the indicated times. After incubation with CCK-8 reagent for 2 hours at 37°C, the absorbance was measured at 450 nm wavelength using a microplate reader (Biotek). Experiments were performed in triplicate and repeated at least three times. Cell viability percentages of treated cells were compared with untreated cell viability, which was normalized as 100%. The half-maximal inhibitory concentrations (IC50 value) were calculated using GraphPad Prism software (GraphPad Software Inc).

Apoptosis assay. Apoptotic cells were identified by staining with FITC-labelled annexin V and propidium iodide using a FITC annexin V apoptosis detection kit (BD Biosciences) according to the manufacturer's instructions. The cells were stained with annexin V-FITC and propidium iodide in annexin V binding buffer for 15 min on ice, then analyzed by flow cytometry using CytoFLEX (Beckman Coulter), and data were analyzed using FlowJo software.

TUNEL assay. DNA fragmentation, which is indicative of apoptosis, was examined using the terminal deoxynucleotidyl transferase-mediated dUTP nick-end labeling method (TUNEL). The TUNEL assay was performed using an in situ cell death detection kit (Roche Molecular Diagnotics) according to the instructions of the manufacturer. Briefly, cells were fixed in 4% paraformaldehyde at room temperature for 1h, then rinsed with phosphate-buffered saline (PBS). The cells were incubated with 3% H_2O_2 (in methanol) at room temperature for 10 min, then rinsed with PBS. The cells were permeated with 0.1% Triton X-100 for 2 min on ice. TUNEL enzyme and label solution were mixed and applied to the prepared cell climbing slices, which were incubated in a humidified chamber for 1 h at 37°C. Slices were thoroughly rinsed with PBS, counterstained with DAPI for nuclear staining and analyzed in a drop of PBS using a fluorescence microscope. The nuclei of apoptotic cells fluoresced green (stained with FITC fluorescein-dUTP). The TUNEL positive cells (apoptotic cells) were counted. Three fields in each section were measured. The percentage of apoptotic cells was quantified by dividing the number of green cells by the total cell number x 100%.

Mitochondrial isolation. Mitochondria were isolated with a mitochondria isolation kit for cultured cells (Thermo Fisher Scientific) according to the manufacturer's instructions. Mitochondria were isolated under sterile conditions at 4°C.

Transfection. PRSS23 (NM_001293180.1) and IL24 (NM_006850.3) overexpression and control vectors were designed and provided by GeneCopoeia, and siRNA specific for PRSS23 (siPRSS23-1) (5'-CCCAGATTTGCTATTGGATTA-3'), (siPRSS23-2) (5'-CAAGCAATATCTGTCTTAT-3'), IL24 (siIL24-1) (5'-ACAAUAGAACAGUUGAAGUCATT-3'), (siIL24-2) (5'-CUGGAUGCAGAAAUUCUACAATT-3'), MKK3 (siMKK3-1) (5'-CAGAAACTTTGAGGTGGAGGCTGAT-3'), MKK3 (siMKK3-2) (5'-CCGAGTTTGTGGACTTCACTGCTCA-3'), MKK4 (siMKK4-1) (5'- CAACTTGTGCCTTACGAAGGA-3'), MKK4 (siMKK4-2) (5'-CCAAAGTGGAATAGTGTATTT-3'), MKK6 (siMKK6-1) (5'- GAGCTAATGCAACATCCATTT-3'), MKK6 (siMKK6-2) (5'- GGATCCGAGCCACAGTAAATA-3'), MKK6 (siMKK6-3) (5'- CAATGCTCTCGGTCAAGTGAA-3') and the non-targeting siRNA control (5'-UUCUCCGAACGUGUCACGUTT-3') were purchased from GenePharma (China). Transfection of plasmids or siRNA into cells using Lipofectamine 3000 (Thermo Fisher

Scientific) was performed according to the manufacturer's instructions. Cells were harvested for western blotting analysis to verify the expression of targeted genes 72 h after transfection.

RNA-seq analysis. GCSCs were treated with or without tipranavir (20 μM) for 24 h, and the total RNA was extracted and purified using TRIzol reagent (Life Technologies) according to the manufacturer's instructions. RNA quantitation and quality control were performed using a Bioanalyzer 2100 (Agilent Technologies). Construction of stranded RNA-seq libraries for high-throughput sequencing was carried out on an Illumina Novaseq 6000 following the manufacturer's protocol. Raw reads passing the Illumina RTA quality filter were pre-processed using FASTQC, version 0.11.2 for quality control of the base sequencing. RNA-seq reads were mapped to the reference genome of Illumina Ensembl genome GRCh37 using STAR version 2.4.2a. Mapped reads were summarized for each gene using RSEM version 1.2.29. Differential expression analysis was performed using edgeR version 3.2.4. *P* values were calculated by the Student's t-test.

Immunoprecipitation. Cell lysates were pre-cleared, incubated in primary antibodies PRSS23 or p38 MAPK antibodies, followed by incubation with protein G beads (GE healthcare). The beads were washed six times by lysis buffer and immunoprecipitates were eluted with SDS sample buffer by boiling for 5 min followed by western blot analysis.

Animal studies. The following animal handling and procedures were approved by the Shenzhen University Animal Care and Use Committee and followed the ARRIVE guidelines. Single-cell GCSC cells were resuspended in PBS medium with Matrigel basement membrane matrix (BD Biosciences) at a 1:1 ratio (total volume 100 μL). Cells (1×10^6 cells) were then were subcutaneously injected into BALB/c nude mice (4–6 weeks old, 16.0 ± 2.0 g). Ten days after inoculation, when the tumor diameter reached about 5 mm, the mice were randomly divided into three groups (5 animals for each group, day 1). Tipranavir was freshly prepared (25 mg/kg/mouse) as described previously [54] with a minor modification. In brief, tipranavir was dissolved in 2% (v/v) ethanol and 10% (v/v) PEG-300 and maintained at 37°C in a water bath. This dissolved solution was then added dropwise to F68 solution (1 mg/ml in normal saline) at 37°C under stirring. The solution was cooled at room temperature before use. The tipranavir solution was intraperitoneally injected every day for 8 days. The control group was injected with the same volume of vehicle (2% ethanol, 10% PEG-300, 1 mg/ml F68). The 5-FU + Cis group was treated with 5-FU (20 mg/kg/mouse) and cisplatin (2 mg/kg/mouse) every day for 8 days. Tumor size and body weight were measured every day. Tumor size was measured using a caliper, and tumor volume was determined by using the formula: $L \times W^2 \times 0.52$, where L is the longest diameter and W is the shortest diameter. After 8 days, all mice were euthanized. Tumors were collected and weighted. Organs including heart, lung, liver, spleen, kidney were harvested, collected and organ coefficients were calculated using the formula: $W_{organ}/W_{Body} \times 100\%$, where W_{organ} is the weight of the organ and W_{Body} is the body weight. The harvested organs were subjected to histological examination using hematoxylin and eosin (H&E) staining.

Statistical analysis. Statistical analyses were performed using GraphPad Prism software (La Jolla, CA, USA). Results are expressed as mean ± SEM, unless indicated otherwise. Groups were compared with either a two-tailed Student t-test for analysis of two groups or a two-way ANOVA to compare multiple groups. Significance was accepted when *P* was less than 0.05.

Results:

Tipranavir inhibits the cell viability of both GCSC and GC cell lines. To discover potential therapeutic drugs targeting GCSCs, we tested four approved HIV-PIs (atazanavir, darunavir, fosamprenavir and tipranavir) in two GCSC cell lines (GCSC1 and GCSC2). Interestingly, we found that low concentrations of tipranavir (0–20 μM) significantly and concentration-dependently inhibited the viability of two GCSC cell lines, whereas other HIV-PIs (atazanavir, darunavir and fosamprenavir) produced little inhibition at low concentrations (Fig. 1a). The half-maximal inhibitory concentration (IC_{50}) values for tipranavir were 4.7 μM in GCSC1 cells and 6.4 μM in GCSC2, and the inhibitory effect was time-dependent (Fig. 1b and Supplementary Fig. 1). Next, we evaluated the effects of 5-fluorouracil (5-FU), cisplatin and tipranavir on two GCSC cell lines. It is well known that CSCs are resistant to conventional chemotherapeutic drugs such as 5-FU and cisplatin. Tipranavir alone or in combination with 5-FU, cisplatin, or 5-FU plus cisplatin significantly inhibited the viability of GCSCs, whereas GCSCs were more resistant to the effects of 5-FU, cisplatin, or 5-FU plus cisplatin treatments (Fig. 1c). These results indicate that tipranavir is more effective at killing GCSCs than chemotherapeutic drugs such as 5-FU and cisplatin, which are the standard first-line chemotherapy regimens for gastric cancer patients. Treatment of GCSCs with tipranavir alone or in combination with 5-FU, cisplatin, or 5-FU plus cisplatin inhibited the growth of GCSCs to a similar degree, suggesting that tipranavir and 5-FU or cisplatin did not act synergistically to inhibit the viability of GCSCs.

The effect of tipranavir on cell viability was also evaluated in a panel of GC cell lines (AGS, HGC-27, MGC-803 and BGC-823 cells) and a normal gastric epithelial cell line (GES-1). As shown in Fig. 1d, tipranavir inhibited growth to a greater extent than 5-FU plus cisplatin in the four GC cell lines. In contrast, GES-1 was insensitive to tipranavir, whereas 5-FU plus cisplatin treatment significantly reduced cell viability; this finding is consistent with the nonspecific off-target toxicities that are associated with 5-FU plus cisplatin (Fig. 1d). These data also indicate that tipranavir induces GC cell death without obvious toxicity in vitro. Furthermore, tipranavir inhibited the viability of various types of human cancer cell lines, including lung (PC9), prostate (PC3), esophageal (KYSE180 and KYSE520), colorectal (HCT116), breast (MDA-MB-231), and liver (Huh7) cancer cells (Supplementary Fig. 2). Interestingly, tipranavir significantly reduced the viability of a paclitaxel-resistant prostate cancer cell line (PC3/Tax) (Supplementary Fig. 2), indicating that tipranavir may kill chemo-resistant cancer cells. Taken together, these data show that tipranavir kills GCSCs, GC cells, and other types of cancer cells without toxicity to normal gastric epithelial cells.

Tipranavir induces GCSCs apoptosis by activating the mitochondrial apoptotic pathway. Tipranavir-treated GCSC1 and GCSC2 cells exhibited morphological changes typical of apoptotic cell death, including cytoplasmic shrinkage, nuclear fragmentation and cell disassembly into apoptotic bodies

(Fig. 2a). In line with this observation, annexin V-FITC and PI staining analyses revealed that tipranavir-treated GCSC1 and GCSC2 cells had a much higher apoptotic rate than control cells (Fig. 2b, c). Moreover, TUNEL assays showed that the apoptotic rate of tipranavir-treated GCSCs was significantly higher than that of control GCSCs, confirming that tipranavir had pro-apoptotic activity (Fig. 2d, e).

Next, we studied the effects of tipranavir on the regulation of apoptotic signaling pathways. The intrinsic or mitochondrial apoptosis pathway involves changes in mitochondrial outer membrane permeabilization (MOMP) [26]. MOMP is controlled by pro- and anti-apoptotic members of the Bcl-2 protein family, which collectively determine cellular death and survival decisions [27, 28]. As shown in Fig. 2f, the pro-apoptotic Bcl-2 proteins Bax and Bak, which are the essential effectors of MOMP, were strongly upregulated in GCSC1 and GCSC2 cells after 72 h of treatment with tipranavir. However, the tipranavir also upregulated two anti-apoptotic proteins, Bcl-2 and Bcl-xL, in GCSC1 and GCSC2 cells. Nevertheless, pro-apoptotic markers including cleaved forms of caspase-9, caspase-7, caspase-3 and PARP were activated in tipranavir-treated GCSCs (Fig. 2f). In line with these results, tipranavir treatment caused the release of cytochrome c from the mitochondria into the cytosol (Fig. 2f). Collectively, these data indicate that tipranavir causes GCSC cell apoptosis by activating the mitochondrial apoptotic pathway. Interestingly, 5-FU plus cisplatin treatment had little effect on the expression of these Bcl-2 family members and pro-apoptotic markers in GCSC1 and GCSC2 cells (Supplementary Fig. 3). Moreover, the protein level of mitochondrial cytochrome c was significantly lower in tipranavir-treated GCSCs than in 5-FU plus cisplatin-treated GCSCs (Supplementary Fig. 3), and whole-cell cytochrome c levels were significantly higher in tipranavir-treated GCSCs (Supplementary Fig. 3). This result indicated that tipranavir is more effective than 5-FU plus cisplatin in inducing apoptosis of GCSCs.

Tipranavir-induced GCSC and GC apoptosis are dependent on PRSS23. To elucidate the molecular basis of apoptosis induced by tipranavir, we performed RNA sequencing (RNA-seq) analysis on GCSCs treated with or without tipranavir (Supplementary Fig. 4). Compared with the expression profile of control GCSCs without tipranavir treatment, 423 genes were up-regulated and 350 genes were down-regulated in tipranavir-treated GCSCs (using an arbitrary cut-off of the signal log ratio ≥ 2.0 or ≤ -2.0; Supplementary Table 1). Notably, we observed a significant reduction of PRSS23 (fold-change = 0.31; Supplementary Table 1), a novel serine protease. GO cellular component analysis ranked this gene highest of all the genes that were down-regulated upon tipranavir treatment (Supplementary Table 2). Proteases play key roles in the mitochondrial apoptotic pathway. PRSS23 is regulated by estrogen receptor α in ER-positive breast cancer cells, and it might be a critical component of estrogen signaling, which affects cell proliferation, survival and apoptosis [29]. A previous study showed that PRSS23 knockdown inhibited gastric cancer cell proliferation and induced apoptosis, indicating that the depletion of PRSS23 confers a strong apoptosis-promoting effect on cancer cells [30]. Therefore, we explored whether PRSS23 is a therapeutic target of tipranavir in GCSCs. In line with our RNA-seq data, qPCR analysis confirmed a 0.28- and 0.24-fold downregulation of PRSS23 in GCSC1 and GCSC2 cells, respectively, upon tipranavir treatment (Fig. 3a). Western blotting analyses showed that tipranavir treatment reduced PRSS23 protein expression in GCSC1 and GCSC2 cells (Fig. 3b) and this effect was concentration-dependent (Fig. 3c). This result indicates that PRSS23 may be indispensable for tipranavir-induced GCSC apoptosis.

To determine whether tipranavir exerts its apoptogenic activity through PRSS23 in GCSCs, we examined the effect of tipranavir on the growth of GCSCs treated with PRSS23-targeting siRNAs. As expected, PRSS23 knockdown significantly reduced the cell viability of GCSC1 (Fig. 3d) and caused GCSC cell apoptosis by activating the pro-apoptotic marker cleaved PARP (Fig. 3f), which were similar to those effects produced by tipranavir treatment on GCSC1 (Fig. 3d, f). Conversely, PRSS23 overexpression in GCSC2 enhanced cell proliferation, rescued the reduction in GCSC cell viability induced by tipranavir (Fig. 3e), and attenuated the tipranavir-induced activation of the mitochondrial apoptotic pathway in GCSCs (Fig. 3g). Moreover, we also investigated whether tipranavir exerted its apoptogenic activity through PRSS23 in GC cell lines. Similar to the results in GCSCs, PRSS23 knockdown significantly reduced the viability of AGS and HGC-27 cells (Fig. 3h), and caused GC cell apoptosis by activating cleaved PARP (Fig. 3i). These results indicate that tipranavir-mediated inhibition of PRSS23 contributes to the proapoptotic effects of tipranavir, and suggest that PRSS23 could be a new therapeutic target for reducing the growth of GCSC and GC cells.

Tipranavir-inhibited PRSS23 induces IL24 expression to promote GCSC apoptosis. We found that tipranavir treatment significantly increased the mRNA level of IL24 (fold change = 6.4; Supplementary Fig. 5), which is a known apoptosis-promoting tumor suppressor in human cancer cells [31, 32]. Moreover, IL24 could target CSCs for death [33, 34]. PRSS23 knockdown enhanced the protein expression of IL24 in GCSCs (Supplementary Fig. 6), so we sought to further investigate its role in tipranavir-induced GCSC apoptosis. Real-time PCR analysis showed that tipranavir treatment increased mRNA expression of IL24 in GCSC1 and GCSC2 cells (Fig. 4a), and western blotting analyses showed that tipranavir increased IL24 protein expression (Fig. 4b) in a concentration-dependent manner in GCSCs (Fig. 4c, d). These results indicate that IL24 may be indispensable for tipranavir-induced GCSC apoptosis. To investigate whether the anti-GCSCs effects of tipranavir are dependent on IL24, we performed siRNA-mediated knockdown of IL24 in GCSC1 and GCSC2 cells. As expected, tipranavir-mediated GCSC apoptosis was inhibited by the expression of two functional siRNAs targeting IL24 (Fig. 4e). The tipranavir-induced expression of mitochondrial apoptotic pathway proteins such as Bax, Bak, cleaved caspase-9, cleaved caspase-7, cleaved caspase-3, and cleaved PARP were strongly inhibited in siRNA-treated cells but not in control cells. The tipranavir-induced cytochrome c efflux from mitochondria was blocked in si-RNA-treated GCSC1 cells (Fig. 4f). Notably, knockdown of IL24 did not alter the expression of the anti-apoptotic proteins Bcl-2 and Bcl-xL in GCSC1 cells treated with tipranavir. This result suggests that the IL24-dependent mitochondrial apoptosis pathway that is activated by tipranavir in GCSCs may be independent of Bcl-2 and Bcl-xL, but dependent upon Bax and Bak. This finding is in line with previous reports showing that Bax and Bak alone were sufficient to induce MOMP [35, 36]. Furthermore, we examined the effects of IL24 overexpression on GCSCs. Ectopic overexpression of IL24 inhibited cell growth and induced apoptosis (Fig. 4g), and also activated the mitochondrial apoptotic pathway in GCSCs (Fig. 4h). Taken together, these results indicate that tipranavir induces GCSC apoptosis by reducing the expression PRSS23, which induces IL24 expression and thereby strongly influences the expression of pro-apoptotic proteins Bax and Bak to activate the mitochondrial apoptotic pathway.

The IL24-dependent mitochondrial apoptotic pathway activated by tipranavir relies on MKK3/p38 MAPK.

A previous study showed that phosphorylated p38 MAPK regulates IL24 expression by altering IL24 mRNA stability [37]. To assess the molecular mechanisms that underlie how IL24 expression is regulated by tipranavir-induced increases in PRSS23 in expression, we first investigated whether tipranavir alters p38 MAPK activation in GCSCs and the effect of p38 MAPK activation on IL24 mRNA expression. Accordingly, western blotting analyses showed that tipranavir increased phosphorylated p38 MAPK in GCSC1 cells (Fig. 5a). Moreover, the p38 MAPK inhibitor SB203580 downregulated IL24 mRNA expression in the absence or presence of tipranavir. Conversely, treatment with the p38 MAPK agonist anisomycin significantly enhanced an increase in IL24 mRNA expression induced by tipranavir (Fig. 5b). Simultaneous inhibition of transcription (using actinomycin D) and inhibition of p38 MAPK (using SB203580) decreased IL24 mRNA expression to a level similar to that observed with actinomycin D treatment alone (Fig. 5c). Treatment with actinomycin D (an RNA polymerase inhibitor) and anisomycin, or tipranavir alone increased IL24 mRNA expression, while combined treatment with SB203580, actinomycin D and tipranavir significantly decreased IL24 mRNA expression (Fig. 5c). Hence, as anticipated, IL24 expression is regulated by phosphorylated p38 MAPK, which alters IL24 mRNA stability in GCSCs.

Next, we determined whether phosphorylation of p38 MAPK can be modulated by PRSS23. Indeed, PRSS23 knockdown activated p38 MAPK and increased the level of phosphorylated p38 MAPK in GCSCs (Fig. 5d). Overexpression of PRSS23 decreased phosphorylated p38 MAPK (Fig. 5d), indicating that PRSS23 regulates the phosphorylation of p38 MAPK.

As p38 MAPK can be phosphorylated by MKK3, MKK6, or MKK4 [38], we next determined which kinase is responsible for the p38 MAPK phosphorylation. We silenced MKK3, MKK4, or MKK6 by siRNA and measured changes in the level of phosphorylated p38 MAPK. Knockdown of MKK3 significantly reduced the level of phosphorylated p38 MAPK; however, knockdown of MKK6 or MKK4 had little effect on the level of phosphorylated p38 MAPK (Supplementary Fig. 7), suggesting that phosphorylation of p38 MAPK is mainly dependent on MKK3. In line with these results, MKK3 knockdown decreased the level of phosphorylated p38 MAPK in tipranavir-untreated GCSCs, without the alteration of the expression of PRSS23 (Fig. 5e), while tipranavir treatment increased the level of phosphorylated p38 MAPK by inhibition of PRSS23 expression (Fig. 5e), and MKK3 depletion impaired the tipranavir-induced up-regulation of phosphorylated p38 MAPK (Fig. 5e), indicating that PRSS23 regulates the level of phosphorylated p38 MAPK via MKK3.

To dissect how PRSS23 modulates the level of phosphorylated p38 MAPK via MKK3 in GCSCs, we investigated the interactions between PRSS23 and MKK3, or p38 MAPK and MKK3. In GCSCs, phophorylated MKK3 (p-MKK3) binds predominately to PRSS23 rather than p38 MAPK (Fig. 5f), which leads to the presence of unphosphorylated p38 MAPK. However, tipranavir treatment reduces the expression of PRSS23, which releases phosphorylated MKK3 and allows it to interact with and activate p38 MAPK (Fig. 5f). In GC cells, phophorylated MKK3 (p-MKK3) binds predominately to p38 MAPK with or without tipranavir treatment, indicating that PRSS23-induced GC apoptosis is not dependent on the MKK3/p38 MAPK pathway (Fig. 5g). Overall, these results suggest that tipranavir-induced activation of

the IL24-dependent mitochondrial apoptotic pathway relies on the PRSS23/MKK3/p38 signaling cascade in GCSCs.

Tipranavir inhibits GCSC-derived tumor growth in vivo without apparent toxicity. To explore the anti-tumor potential of tipranavir in vivo, nude mice bearing GCSC tumors were treated intraperitoneally with tipranavir (25 mg/kg), 5-FU plus cisplatin (5-FU: 20 mg/kg, cisplatin: 2 mg/kg), or vehicle (i.p.) once every day for 8 days, receiving eight treatments (Fig. 6a). As shown in Fig. 6b and 6c, GCSC-derived tumors from the tipranavir-treated group were significantly smaller and had a lower tumor weight than tumors from the control and 5-FU plus cisplatin-treated treatment groups. Tipranavir significantly inhibited the growth of subcutaneous GCSC tumors (Fig. 6d; $P < 0.0001$). There was no obvious difference in the growth of GCSC tumors between the 5-FU plus cisplatin treatment group and the control group (Fig. 6d; $P > 0.05$). These results are consistent with our in vitro data which showed that GCSCs are resistant to 5-FU and cisplatin, and suggest that tipranavir could inhibit GCSC-derived tumors more effeminately than standard chemotherapy drugs.

We used histopathology to evaluate the toxicity of tipranavir in vivo. H&E staining results showed no apparent injury to major organs, including the heart, lung, liver, spleen and kidney (Fig. 6e and Supplementary Fig. 8). Measurement of body weights, which respond to the systemic toxicity of drugs, showed that the average body weight in of tipranavir-treated group was similar to that of the control group (Fig. 6f; $P > 0.05$), suggesting that tipranavir did not cause weight loss in mice. However, treatment with 5-FU plus cisplatin caused significant weight loss in mice (Fig. 6f; $P < 0.0001$). Moreover, there was no significant difference in the organ coefficients of the major organs between the tipranavir-treated and control groups, suggesting that tipranavir treatment had no detectable toxic effects on the heart, lung, liver, spleen, and kidney (Fig. 6g). In contrast, treatment with 5-FU plus cisplatin significantly reduced the weight of the spleen, suggesting that this drug combination may impair spleen function (Fig. 6g; $P < 0.001$).

To test whether tipranavir promotes mitochondrial apoptosis by decreasing PRSS23 and inducing IL24 expression in vivo, we evaluated the protein expression of PRSS23, IL24 and apoptotic marker cleaved PARP in tumor samples from tipranavir-treated and control mice. GCSCs-derived tumors from the tipranavir-treated group showed significantly lower expression of PRSS23, and higher expression of IL24 and cleaved PARP than those from the control group (Fig. 6h). This result indicates that tipranavir suppressed gastric tumor growth via the PRSS23/IL24-mediated mitochondrial apoptotic pathway in vivo. Collectively, these data suggest that tipranavir may be an effective anti-tumor drug with little toxicity.

Discussion:

Tipranavir, a non-peptidic HIV-1 protease inhibitor, is an FDA-approved antiviral drug that is used in combination with ritonavir to treat HIV-1 infection. It is advantageous particularly in the management of patients with multi-protease inhibitor-resistant HIV [39–41]. Our current study demonstrates that tipranavir kills GCSC cells and inhibits tumor growth in human GCSCs xenografts without any observable

toxic effects. Moreover, we showed that tipranavir induces GC cell death without cytotoxicity to normal gastric epithelial cells. Emerging evidence supports the notion that conventional chemotherapy targets fast-proliferating tumor cells, leading to the emergence of residual chemo-resistant cells with CSCs-like properties that may cause tumor relapse and metastasis [42]. While killing CSCs may lead to tumor regression, the combined killing of both cancer cells and CSCs may offer the opportunity to cure cancers. The results of the present study suggest that tipranavir could effectively eliminate gastric tumors. Tipranavir is an FDA-approved drug, so repurposing it as an anti-cancer drug would be beneficial for the effective treatment and/or long-term cure for GC patients. Additionally, tipranavir might have broad-spectrum anti-cancer effects, as it inhibited the growth of lung, prostate, esophageal, colorectal, breast, and liver cancer cells. Intriguingly, tipranavir was able to kill paclitaxel-resistant prostate cancer cells, so further studies to investigate its potential in paclitaxel-resistant prostate cancer is warranted.

In the present study, we provide the first evidence that tipranavir induces GCSC death via the IL24-dependent mitochondrial apoptotic pathway. IL24 (also known as melanoma differentiation-associated gene-7; mda-7) is a tumor suppressor gene found in numerous types of cancers [32]. Overexpression of IL24 induces apoptosis in a wide variety of cancer cells without affecting normal human cells [31]. In addition, preclinical and clinical data demonstrate that IL24 is a potent, effective therapeutic agent for cancer treatment [46–48]. In this study, we demonstrated that tipranavir upregulates the expression of IL24, which induces GCSC apoptosis. This finding is consistent with a previous study showing that recombinant human IL24 induces gastric cancer cell apoptosis and suppress tumor growth in vitro and in vivo [49]. However, it is not yet fully understood how IL24 induces tumor-cell apoptosis. Previous studies indicate that IL24 modulates the mitochondrial apoptotic pathway by downregulating the expression of anti-apoptotic proteins such as Bcl-2, Bcl-xL Mcl-1, and upregulating the expression of pro-apoptotic proteins such as Bax, Bak, Bim and Bid [50], thereby increasing the ratio of pro-apoptotic to anti-apoptotic proteins [51]. In this study, we observed a dramatic upregulation of pro-apoptotic proteins, including Bax and Bak, in tipranavir-treated GCSC cells or IL24-overexpressing GCSC cells. Unexpectedly, anti-apoptotic proteins like Bcl-2 and Bcl-xL were also upregulated tipranavir-treated GCSC cells or IL24-overexpressing GCSC cells; this finding is inconsistent with previous reports. Moreover, knockdown of IL24 didn’t alter the level of Bcl-2 and Bcl-xL in tipranavir-treated GCSC cells, but significantly reduced the expression of Bax and Bak, suggesting that the IL24-mediated mitochondrial apoptotic pathway is mainly dependent on Bax and Bak. In agreement with this finding, genetic deletion of all Bcl-2 proteins and reintroduction of Bax alone was sufficient to induce MOMP [36]. It seems that the mechanism by which IL24-Bax/Bak induces apoptosis in GCSC is different from the previous reported mechanisms of IL24-mediated apoptosis in other cells. Further studies to elucidate the molecular mechanisms that underlie how IL24 regulates Bax/Bak in GCSCs will improve our understanding of the biological function of GCSCs, and possibly lead to new therapies targeting GCSCs. Taken together, our findings suggest that the IL24-induced GCSC apoptosis elicited by tipranavir can be attributed to the activity of Bax and Bak, which shifts the balance of cell fate survival to death.

How does the tipranavir-mediated decrease PRSS23 expression regulate IL24 expression in GCSCs? Previous studies demonstrated that AP1 and CEBPβ are involved in the transcriptional control of IL24

expression [52]. Based on our RNA-seq data (Supplementary Table 1) and real-time PCR analysis (Supplementary Fig. 9a), we found that tipranavir treatment significantly upregulated the expression of the CEBPβ gene. However, western blotting analysis revealed that tipranavir or PRSS23 knockdown reduced the protein expression of CEBPβ (Supplementary Fig. 9b, 9c). Additionally, our results also demonstrated that IL24 expression isn't modulated by AP1. Mechanistically, we found that activation of the IL24-mediated mitochondrial apoptotic pathway depended on the phosphorylation of p38 MAPK by MKK3. Activated p38 MAPK can regulate IL24 expression through a mechanism involving mRNA stabilization [37], and p38 MAPK can be phosphorylated by MKK3/MKK6, or MKK4 [38]. In this study, we demonstrated that in GCSCs, MKK3/p38 MAPK activation is modulated by PRSS23 expression. Unlike the direct link between MKK3/p38 MAPK that is not depended on PRSS23 in GC cells, our findings reveal that in GCSCs, the IL24-mediated mitochondrial apoptotic pathway is regulated by a rare and complex mechanism. Within this CSCs-specific mechanism of apoptotic regulatory networks, CSCs could be more resistant than GCs to apoptosis and cell death induced by extracellular stimuli. In this perspective, our findings could provide a potentially safe, effective therapeutic strategy to kill GCSCs.

In this study, we demonstrated that tipranavir exerts its apoptogenic activity by decreasing the expression of PRSS23 in both GCSC and GC cells. PRSS23 is a novel serine protease, initially identified in mouse ovary [45]. However, few studies on the structure and function of PRSS23 have been conducted. Although molecular docking studies showed that PRSS23 is not a direct target of tipranavir (data not shown), it is plausible that tipranavir's functional target is PRSS23. The expression of PRSS23 was concentration-dependently inhibited by tipranavir, and inhibition of PRSS23 — either by siRNA knockdown or tipranavir — produced similar apoptotic effects in both GCSC and GC cells. Conversely, PRSS23 overexpression in GCSCs protected cells from tipranavir-mediated apoptosis. Mechanistically, PRSS23 interacts with phosphorylated MKK3, and interferes with the binding of phosphorylated MKK3 to p38 MAPK in GCSCs. Depletion of PRSS23 by tipranavir releases MKK3, which activates p38 MAPK, resulting in activation of the IL24-dependent mitochondrial apoptotic pathway in GCSC cells. However,, PRSS23 doesn't interact with phosphorylated MKK3 in GC cells, and the detail mechanism that tipranavir-induced GC cells apoptosis needs to be further investigated.

Clinically targeting the MKKs/p38 MAPK pathway is challenging because of the intrinsic pleiotropic nature of MKKs and p38 MAPK. Targeting PRSS23 could represent an effective and potentially safe therapeutic strategy to kill gastric cancer stem cells. The key molecule(s) involved in GCSC survival are still poorly understood. To the best of our knowledge, this is the first study to identify a potential molecular drug target that is expressed by both GCSC and GC cells. Recently, PRSS23 knockdown was shown to inhibit GC cell proliferation and induce apoptosis by inhibiting EIF2 signaling [30]. Our findings suggest that PRSS23 could represent a selective, safe, and effective way of targeting GCSCs. Moreover, PRSS23-targeted therapy in combination with drugs that act on other targets such as EIF4E may offer an attractive approach to combating gastric cancer.

Conclusions:

In summary, our present study demonstrates that tipranavir induces GCSC apoptosis via the PRSS23/MKK3/p38MAPK–IL24–Bax/Bak mitochondrial apoptotic pathway (Fig. 7). Moreover, tipranavir induced GC cell death without cytotoxicity to normal cells. Our findings not only provide evidence that by targeting both GCSC and GC cells, tipranavir could be a promising gastric cancer drug but also provide the first evidence that the PRSS23–IL24-mediated mitochondrial apoptotic pathway is a new target for the treatment of gastric cancer.

Abbreviations

GCSCs Gastric cancer stem cells

GC gastric cancer

IL interleukin

5-FU 5-fluorouracil

CSCs Cancer stem cells

GAC gastric adenocarcinoma

HIV human immunodeficiency virus

PIs protease inhibitors

CCK-8 cell counting kit-8

IC_{50} half-maximal inhibitory concentrations

TUNEL terminal deoxynucleotidyl transferase-mediated dUTP nick-end labeling

PBS phosphate-buffered saline

H&E hematoxylin and eosin

MOMP mitochondrial outer membrane permeabilization

p-MKK3 phophorylated MKK3

mda-7 melanoma differentiation-associated gene-7

Declarations

Ethics approval and consent to participate

This study was approved by the institutional review board of Shenzhen University. Informed consents were obtained for the original work that produced human tissue samples.

Consent for publication

All subjects have written informed consent.

Availability of data and materials

The data that support the findings of this study are available from the corresponding author upon reasonable request.

Competing Interests

The authors declare that they have no competing interests.

Funding

This work was supported by grants from the National Key R&D Program of China (2017YFA0503900), the National Natural Science Foundation of China (82173003), the Science and Technology Foundation of Shenzhen (JCYJ20200109113810154), the Science and Technology Program of Guangdong Province in China (2019B030301009), the Industry and Information Technology Foundation of Shenzhen (20180309100135860), the SZU Top Ranking Project (86000000210), the Guangdong Basic and Applied Basic Research Foundation (2020A1515010989 and 2018A030310586), and the Medical Scientific Research Foundation of Guangdong Province (A2019405).

Authors' contributions

Conceptualization: J.X., and L.F.; Methodology: J.X., Y.L., X.T., and L.F.; Investigation: J.X, Y.L., X.T., and T.C.; Writing: J.X., and L.F.; Funding acquisition: J.X., and L.F.; Resources: B.L.; Supervision: J.X., and L.F.

Acknowledgments

We acknowledge Dr Xianming Mo (Sichuan University) for providing the GCSC cells. We thank Dr Xiangwei Wang and Dr Yuqi Wu (Shenzhen University General Hospital) for providing the PC3/Tax cells. We also thank Dr Wen Su (Shenzhen University) for her help in histological examination.

References

1. Bray F, Ferlay J, Soerjomataram I, Siegel RL, Torre LA, Jemal A. Global cancer statistics 2018: GLOBOCAN estimates of incidence and mortality worldwide for 36 cancers in 185 countries. CA Cancer J Clin. 2018;68(6):394–424.
2. IARC, WHO. Cancer fact sheets, stomach. 2018; https://gco.iarc.fr/today/data/factsheets/cancers/7-Stomach-fact-sheet.pdf (accessed Oct 15, 2020).

3. Cao W, Chen HD, Yu YW, Li N, Chen WQ. Changing profiles of cancer burden worldwide and in China: a secondary analysis of the global cancer statistics 2020. Chin Med J (Engl). 2021;134(7):783–791.
4. Van Cutsem E, Sagaert X, Topal B, Haustermans K, Prenen H. Gastric cancer. Lancet. 2016;388(10060):2654–2664.
5. Ajani JA, Lee J, Sano T, Janjigian YY, Fan D, Song S. Gastric adenocarcinoma. Nat Rev Dis Primers. 2017;3:17036.
6. Smyth EC, Verheij M, Allum W, Cunningham D, Cervantes A, Arnold D. Gastric cancer: ESMO Clinical Practice Guidelines for diagnosis, treatment and follow-up. Ann Oncol. 2016;27 (suppl 5):v38–49.
7. Muro K, Van Cutsem E, Narita Y, Pentheroudakis G, Baba E, Li J, Ryu MH, Zamaniah WIW, Yong WP, Yeh KH, Kato K, Lu Z, Cho BC, Nor IM, Ng M, Chen LT, Nakajima TE, Shitara K, Kawakami H, Tsushima T, Yoshino T, Lordick F, Martinelli E, Smyth EC, Arnold D, Minami H, Tabernero J, Douillard JY. Pan-Asian adapted ESMO clinical practice guidelines for the management of patients with metastatic gastric cancer: a JSMO-ESMO initiative endorsed by CSCO, KSMO, MOS, SSO and TOS. Ann Oncol. 2019;30:19–33.
8. Ajani JA, D'Amico TA, Almhanna K, Bentrem DJ, Chao J, Das P, Denlinger CS, Fanta P, Farjah F, Fuchs CS, Gerdes H, Gibson M, Glasgow RE, Hayman JA, Hochwald S, Hofstetter WL, Ilson DH, Jaroszewski D, Johung KL, Keswani RN, Kleinberg LR, Korn WM, Leong S, Linn C, Lockhart AC, Ly QP, Mulcahy MF, Orringer MB, Perry KA, Poultsides GA, Scott WJ, Strong VE, Washington MK, Weksler B, Willett CG, Wright CD, Zelman D, McMillian N, Sundar H. Gastric Cancer, Version 3.2016, NCCN Clinical Practice Guidelines in Oncology. J Natl Compr Canc Netw. 2016;14(10):1286–1312.
9. Warschkow R, Baechtold M, Leung K, Schmied BM, Nussbaum DP, Gloor B, Blazer Iii DG, Worni M. Selective survival advantage associated with primary tumor resection for metastatic gastric cancer in a Western population. Gastric Cancer. 2018;21(2):324–337.
10. Wagner AD, Syn NL, Moehler M, Grothe W, Yong WP, Tai BC, Ho J, Unverzagt S. Chemotherapy for advanced gastric cancer. Cochrane Database Syst Rev. 2017;8(8):CD004064.
11. Lordick F, Shitara K, Janjigian YY. New agents on the horizon in gastric cancer. Ann Oncol. 2017;28(8):1767–1775.
12. Batlle E, Clevers H. Cancer stem cells revisited. Nat Med. 2017;23:1124–1134.
13. Beck B, Blanpain C. Unravelling cancer stem cell potential. Nat Rev Cancer. 2013;13(10):727–738.
14. Pützer BM, Solanki M, Herchenröder O. Advances in cancer stem cell targeting: How to strike the evil at its root. Adv Drug Deliv Rev. 2017;120:89–107.
15. Kaiser J. The cancer stem cell gamble. Science. 2015;347(6219):226–229.
16. Saygin C, Matei D, Majeti R, Reizes O, Lathia JD. Targeting Cancer Stemness in the Clinic: From Hype to Hope. Cell Stem Cell. 2019;24(1):25–40.
17. Takaishi S, Okumura T, Tu S, Wang SS, Shibata W, Vigneshwaran R, Gordon SA, Shimada Y, Wang TC. Identification of gastric cancer stem cells using the cell surface marker CD44. Stem Cells. 2009;27(5): 1006–1020.

18. Chen T, Yang K, Yu J, Meng W, Yuan D, Bi F, Liu F, Liu J, Dai B, Chen X, Wang F, Zeng F, Xu H, Hu J, Mo X. Identification and expansion of cancer stem cells in tumor tissues and peripheral blood derived from gastric adenocarcinoma patients. Cell Res. 2012;22(1):248–258.
19. Brungs D, Aghmesheh M, Vine KL, Becker TM, Carolan MG, Ranson M. Gastric cancer stem cells: evidence, potential markers, and clinical implications. J Gastroenterol. 2016;51(4):313–326.
20. Fu L, Bu L, Yasuda T, Koiwa M, Akiyama T, Uchihara T, Baba H, Ishimoto T. Gastric Cancer Stem Cells: Current Insights into the Immune Microenvironment and Therapeutic Targets. Biomedicines. 2020;8(1):7.
21. Lytle NK, Barber AG, Reya T. Stem cell fate in cancer growth, progression and therapy resistance. Nat Rev Cancer. 2018;18(11):669–680.
22. Koltai T. Nelfinavir and other protease inhibitors in cancer: mechanisms involved in anticancer activity. F1000Res. 2015;4:9.
23. Moreau P, Richardson PG, Cavo M, Orlowski RZ, San Miguel JF, Palumbo A, Harousseau JL. Proteasome inhibitors in multiple myeloma: 10 years later. Blood. 2012;20(5):947–959.
24. Gills JJ, Lopiccolo J, Tsurutani J, Shoemaker RH, Best CJ, Abu-Asab MS, Borojerdi J, Warfel NA, Gardner ER, Danish M, Hollander MC, Kawabata S, Tsokos M, Figg WD, Steeg PS, Dennis PA. Nelfinavir, A lead HIV protease inhibitor, is a broad-spectrum, anticancer agent that induces endoplasmic reticulum stress, autophagy, and apoptosis in vitro and in vivo. Clin Cancer Res. 2007;13(17):5183–5194.
25. Rengan R, Mick R, Pryma DA, Lin LL, Christodouleas J, Plastaras JP, Simone CB 2nd, Gupta AK, Evans TL, Stevenson JP, Langer CJ, Kucharczuk J, Friedberg J, Lam S, Patsch D, Hahn SM, Maity A. Clinical Outcomes of the HIV Protease Inhibitor Nelfinavir With Concurrent Chemoradiotherapy for Unresectable Stage IIIA/IIIB Non-Small Cell Lung Cancer: A Phase 1/2 Trial. JAMA Oncol. 2019;5(10):1464–1472.
26. Bock FJ, Tait SWG. Mitochondria as multifaceted regulators of cell death. Nat Rev Mol Cell Biol. 2020;21(2):85–100.
27. Walensky LD. Targeting BAX to drug death directly. Nat Chem Biol. 2019;15(7):657–665.
28. Singh R, Letai A, Sarosiek K. Regulation of apoptosis in health and disease: the balancing act of BCL-2 family proteins. Nat Rev Mol Cell Biol. 2019;20(3):175–193.
29. Chan HS, Chang SJ, Wang TY, Ko HJ, Lin YC, Lin KT, Chang KM, Chuang YJ. Serine protease PRSS23 is upregulated by estrogen receptor α and associated with proliferation of breast cancer cells. PLoS One. 2012;7(1):e30397.
30. Han B, Yang Y, Chen J, He X, Lv N, Yan R. PRSS23 knockdown inhibits gastric tumorigenesis through EIF2 signaling. Pharmacol Res. 2019;142:50–57.
31. Emdad L, Bhoopathi P, Talukdar S, Pradhan AK, Sarkar D, Wang XY, Das SK, Fisher PB. Recent insights into apoptosis and toxic autophagy: The roles of MDA-7/IL-24, a multidimensional anti-cancer therapeutic. Semin Cancer Biol. 2020;66:140–154.

32. Menezes ME, Bhoopathi P, Pradhan AK, Emdad L, Das SK, Guo C, Wang XY, Sarkar D, Fisher PB. Role of MDA-7/IL-24 a Multifunction Protein in Human Diseases. Adv Cancer Res. 2018;138:143–182.
33. Bhutia SK, Das SK, Azab B, Menezes ME, Dent P, Wang XY, Sarkar D, Fisher PB. Targeting breast cancer-initiating/stem cells with melanoma differentiation-associated gene-7/interleukin-24. Int J Cancer. 2013;133(11):2726–2736.
34. Kim JY, Kim JC, Lee JY, Park MJ. Oct4 suppresses IR induced premature senescence in breast cancer cells through STAT3- and NF κB-mediated IL 24 production. Int J Oncol. 2018;53(1):47–58.
35. Chen HC, Kanai M, Inoue-Yamauchi A, Tu HC, Huang Y, Ren D, Kim H, Takeda S, Reyna DE, Chan PM, Ganesan YT, Liao CP, Gavathiotis E, Hsieh JJ, Cheng EH. An interconnected hierarchical model of cell death regulation by the BCL-2 family. Nat Cell Biol. 2015;17(10):1270–1281.
36. O'Neill KL, Huang K, Zhang J, Chen Y, Luo X. Inactivation of prosurvival Bcl-2 proteins activates Bax/Bak through the outer mitochondrial membrane. Genes Dev. 2016;30(8):973–988.
37. Otkjaer K, Holtmann H, Kragstrup TW, Paludan SR, Johansen C, Gaestel M, Kragballe K, Iversen L. The p38 MAPK regulates IL-24 expression by stabilization of the 3' UTR of IL-24 mRNA. PLoS One. 2010;5(1):e8671.
38. Cuadrado A, Nebreda AR. Mechanisms and functions of p38 MAPK signalling. Biochem J. 2010;429(3):403–417.
39. Back NK, van Wijk A, Remmerswaal D, van Monfort M, Nijhuis M, Schuurman R, Boucher CA. In-vitro tipranavir susceptibility of HIV-1 isolates with reduced susceptibility to other protease inhibitors. AIDS. 2000;14(1):101–102.
40. Larder BA, Hertogs K, Bloor S, van den Eynde CH, DeCian W, Wang Y, Freimuth WW, Tarpley G. Tipranavir inhibits broadly protease inhibitor-resistant HIV-1 clinical samples. AIDS. 2000;14(13):1943–1948.
41. Rusconi S, La Seta Catamancio S, Citterio P, Kurtagic S, Violin M, Balotta C, Moroni M, Galli M, d'Arminio-Monforte A. Susceptibility to PNU-140690 (Tipranavir) of human immunodeficiency virus type 1 isolates derived from patients with multidrug resistance to other protease inhibitors. Antimicrob Agents Chemother. 2000;44(5):1328–1332.
42. Clarke MF. Clinical and Therapeutic Implications of Cancer Stem Cells. N Engl J Med. 2019;380(23):2237–2245.
43. Dasari S, Tchounwou PB. Cisplatin in cancer therapy: molecular mechanisms of action. Eur J Pharmacol. 2014;740:364–378.
44. Longley DB, Harkin DP, Johnston PG. 5-fluorouracil: mechanisms of action and clinical strategies. Nat Rev Cancer. 2003;3(5):330–338.
45. Miyakoshi K, Murphy MJ, Yeoman RR, Mitra S, Dubay CJ, Hennebold JD. The identification of novel ovarian proteases through the use of genomic and bioinformatic methodologies. Biol Reprod. 2006;75(6):823–835.
46. Fisher PB, Gopalkrishnan RV, Chada S, Ramesh R, Grimm EA, Rosenfeld MR, Curiel DT, Dent P. mda-7/IL-24, a novel cancer selective apoptosis inducing cytokine gene: from the laboratory into the

clinic. Cancer Biol Ther. 2003;2(4 Suppl 1):S23-37.

47. Tong AW, Nemunaitis J, Su D, Zhang Y, Cunningham C, Senzer N, Netto G, Rich D, Mhashilkar A, Parker K, Coffee K, Ramesh R, Ekmekcioglu S, Grimm EA, van Wart Hood J, Merritt J, Chada S. Intratumoral injection of INGN 241, a nonreplicating adenovector expressing the melanoma-differentiation associated gene-7 (mda-7/IL24): biologic outcome in advanced cancer patients. Mol Ther. 2005;11(1):160–172.
48. Cunningham CC, Chada S, Merritt JA, Tong A, Senzer N, Zhang Y, Mhashilkar A, Parker K, Vukelja S, Richards D, Hood J, Coffee K, Nemunaitis J. Clinical and local biological effects of an intratumoral injection of mda-7 (IL24; INGN 241) in patients with advanced carcinoma: a phase I study. Mol Ther. 2005;11(1):149–159.
49. Yan S, Zhang H, Xie Y, Sheng W, Xiang J, Ye Z, Chen W, Yang J. Recombinant human interleukin-24 suppresses gastric carcinoma cell growth in vitro and in vivo. Cancer Invest. 2010;28(1):85–93.
50. Menezes ME, Bhatia S, Bhoopathi P, Das SK, Emdad L, Dasgupta S, Dent P, Wang XY, Sarkar D, Fisher PB. MDA-7/IL-24: multifunctional cancer killing cytokine. Adv Exp Med Biol. 2014;818:127–153.
51. Pei DS, Yang ZX, Zhang BF, Yin XX, Li LT, Li HZ, Zheng JN. Enhanced apoptosis-inducing function of MDA-7/IL-24 RGD mutant via the increased adhesion to tumor cells. J Interferon Cytokine Res. 2012;32(2):66–73.
52. Madireddi MT, Dent P, Fisher PB. AP-1 and C/EBP transcription factors contribute to mda-7 gene promoter activity during human melanoma differentiation. J Cell Physiol. 2000;185:36–46.
53. Wu Y, Liu X, Qin Z, Hu L, Wang X. Low-frequency ultrasound enhances chemotherapy sensitivity and induces autophagy in PTX-resistant PC-3 cells via the endoplasmic reticulum stress-mediated PI3K/Akt/mTOR signaling pathway. Onco Targets Ther. 2018;11:5621–5630.
54. Chai GH, Xu Y, Chen SQ, Cheng B, Hu FQ, You J, Du YZ, Yuan H. Transport Mechanisms of Solid Lipid Nanoparticles across Caco-2 Cell Monolayers and their Related Cytotoxicology. ACS Appl Mater Interfaces. 2016;8(9):5929–5940.

Figures

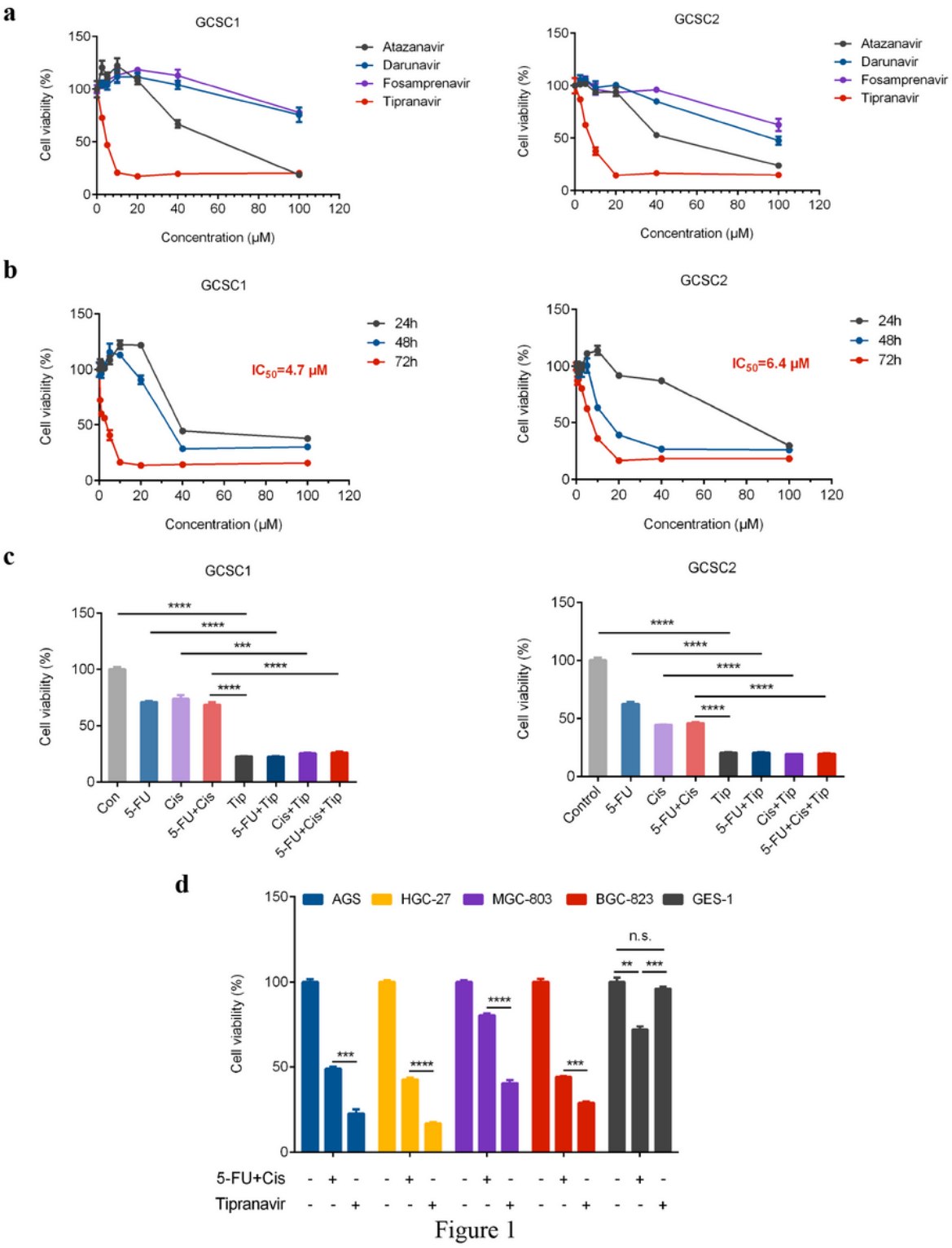

Figure 1

Figure 1

Tipranavir reduces the viability of GCSCs and other cancer cells.

(**a**) The effect of different concentrations of four anti-HIV drugs (atazanavir, darunavir, fosamprenavir and tipranavir) on the viability of two GCSC cell lines (GCSC1 and GCSC2). GCSC1 and GCSC2 cells were treated with atazanavir, darunavir, fosamprenavir, or tipranavir at the indicated concentrations for 72 hr.

Cell viability was analyzed using a CCK-8 assay and is represented as the percentage of the vehicle. Error bars represent the mean ± SEM, n = 3.

(**b**) The viability of GCSC1 and GCSC2 cells treated with the indicated concentrations of tipranavir for 24, 48, or 72 hr. Cell viability was analyzed using a CCK-8 assay and is represented as the percentage of the vehicle. Error bars represent the mean ± SEM, n = 3. The IC_{50} value for 72 hr tipranavir treatment was calculated using GraphPad Prism software.

(**c**) The viability of GCSC1 and GCSC2 cells after treatment with control, 5-FU (2.5 μM), cisplatin (Cis, 4 μM), 5-FU plus cisplatin (5-FU+Cis), tipranavir (Tip, 20 μM), 5-FU plus tipranavir (5-FU+Tip), cisplatin plus tipranavir (Cis+Tip), 5-FU, cisplatin and tipranavir (5-FU+Cis +Tip) for 72 hr measured using a CCK-8 assay. The viability of tipranavir-treated GCSC1 and GCSC2 cells was significantly lower than cells that were not treated with tipranavir. The viability of tipranavir-treated GCSC1 and GCSC2 cells was also significantly lower than GCSC1 and GCSC2 cells treated with 5-FU+Cis. Error bars represent the mean ± SEM, n = 3. *** $P < 0.001$; **** $P < 0.0001$.

(**d**) The viability after treatment with tipranavir (20 μM), 5-FU plus cisplatin (5-FU+Cis, 5-FU: 2.5 μM; Cis: 4 μM) or control in GC cell lines (AGS, HGC-27, MGC-803 and BGC-823 cells) and a normal gastric epithelial cell line (GES-1) at 72 hr assessed using a CCK-8 assay. The viability of each GC cell line treated with tipranavir was significantly lower than the same cell line treated with 5-FU+Cis. There was no difference in the viability of tipranavir-treated GES-1 cells compared with control; the viability in 5-FU+Cis-treated GES-1 cells was significantly lower than the viability of the control group. Error bars represent mean ± SEM, n = 3. ** $P < 0.01$; *** $P < 0.001$; **** $P < 0.0001$; n.s., $P > 0.05$.

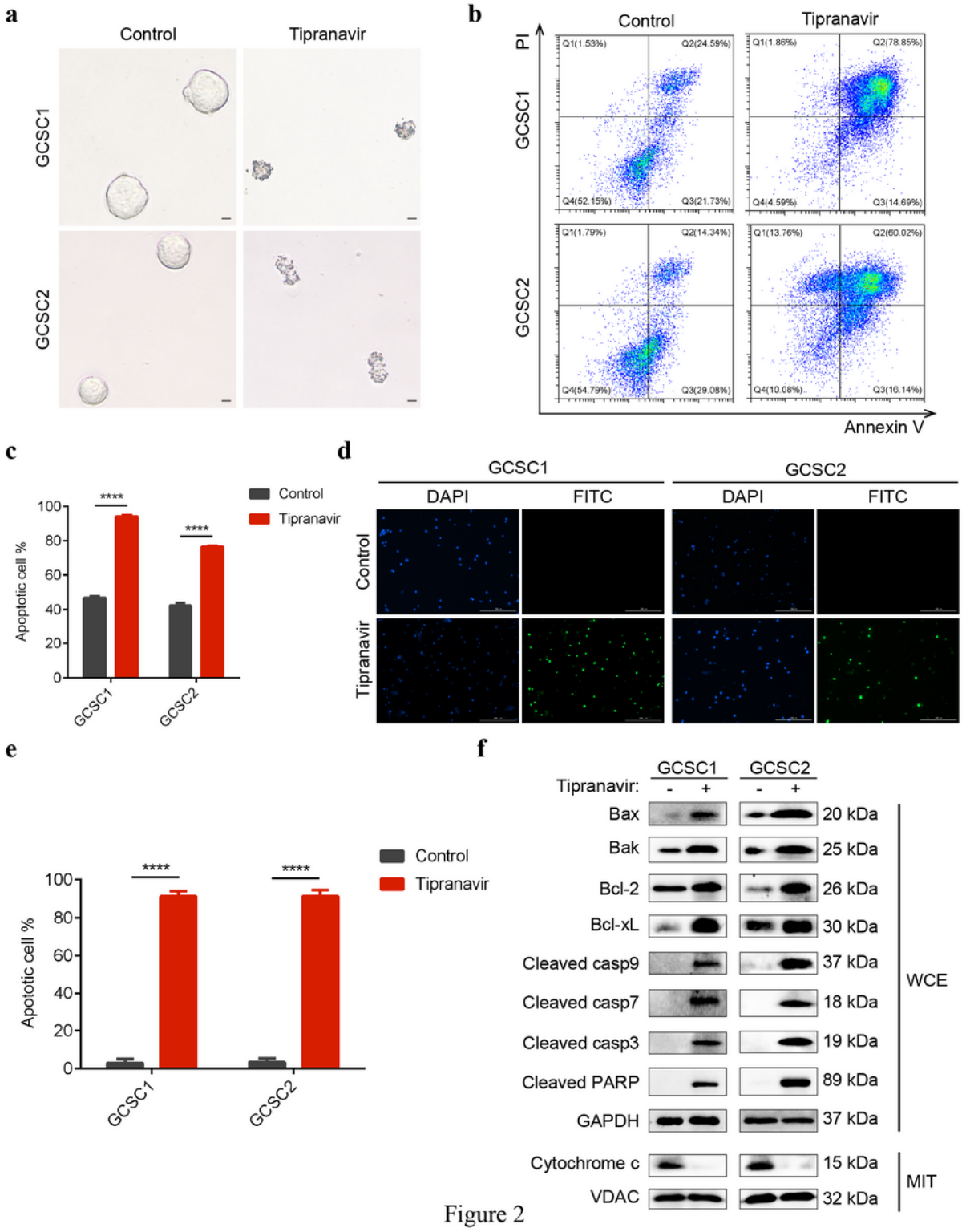

Figure 2

Figure 2

Tipranavir induces apoptosis of GCSCs via the mitochondrial pathway.

(**a**) Representative cell morphology of GCSC1 and GCSC2 cells treated with or without tipranavir for 48 hr. Scale bar, 50 μm. Representative data shown are one of three independent biological repeat experiments

(**b**) Flow cytometry analysis of GCSC1 and GCSC2 cells treated with or without tipranavir for 48 hr. Cell apoptosis of GCSCs was measured by annexin V-FITC/PI staining and flow cytometry.

(**c**) A summary of the apoptotic index showing that tipranavir treatment increased apoptosis of GCSC cells. The values indicate the mean ± SEM of three separate experiments. **** $P < 0.0001$.

(**d**) Representative images of GCSCs treated with or without tipranavir for 48 hr following by TUNEL staining. Green: apoptotic cells; blue: DAPI staining. Scale bar, 200 μm.

(**e**) The percentage of apoptotic cells. The percentage of apoptotic cells in tipranavir-treated groups was significantly higher than that in the control groups in GCSC1 and GCSC2 cells. The values indicate the mean ± SEM of four separate experiments. **** $P < 0.0001$.

(**f**) The expression of Bax, Bak, Bcl-2, Bcl-xL, cleaved caspase-9, cleaved caspase-7, cleaved caspase-3, cleaved PARP in the whole-cell extract (WCE), and cytochrome c in the mitochondria (MIT) from GCSC1 and GCSC2 cells with or without tipranavir treatment for 48 hr was detected by western blot analysis. GAPDH or VDAC was used as a loading control.

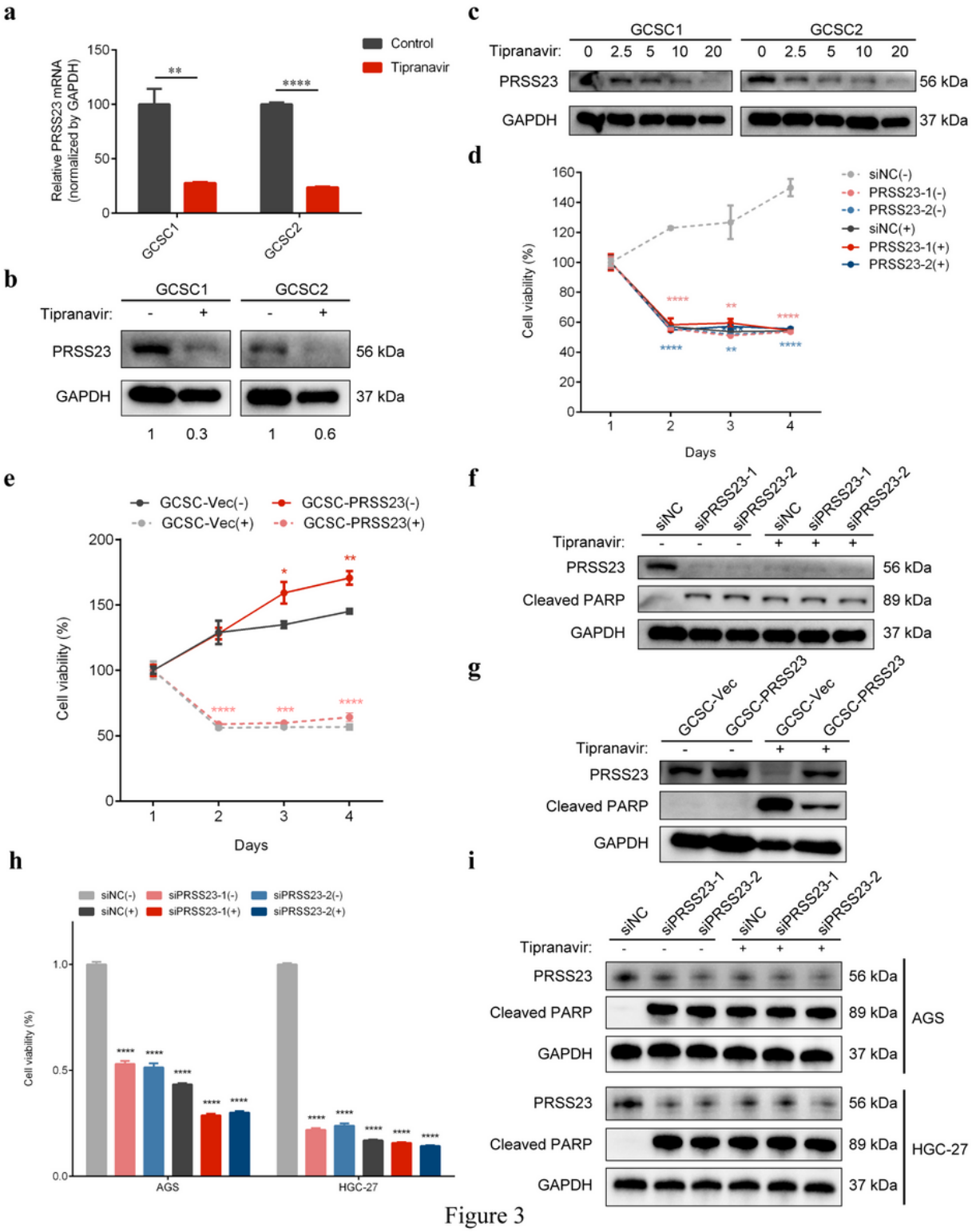

Figure 3

Figure 3

Tipranavir-induced GCSC and GC apoptosis are dependent on PRSS23.

(**a**) Relative mRNA levels of PRSS23 in GCSC1 and GCSC2 cells treated with or without tipranavir for 24 hr. GAPDH was used as an internal control. Error bars represent the mean ± SEM, n = 3. ** P < 0.01; **** P < 0.0001.

(**b**) The expression of PRSS23 in GCSC1 and GCSC2 with or without tipranavir treatment for 48 hr was detected by western blot analysis. Quantitative data of the relative protein expression is illustrated. GAPDH was used as a loading control.

(**c**) The expression of PRSS23 in GCSC1 and GCSC2 cells treated with the indicated concentrations of tipranavir for 48 hr was detected by western blot analysis. GAPDH was used as a loading control.

(**d**) The cell viability after treatment with or without tipranavir in control GCSC1 cells (siNC) and PRSS23-silenced GCSC1 cells (siPRSS23-1/siPRSS23-2). A CCK-8 assay was used to measure cell viability at the indicated times. Tipranavir was added from day 1. Error bars represent the mean ± SEM, n = 3. ** P < 0.01; **** P < 0.0001.

(**e**) The viability of control GCSC2 cells (GCSC-Vec) and PRSS23-overexpressing GCSC2 cells (GCSC-PRSS23). Cell viability was assessed using a CCK-8 assay at the indicated times. Tipranavir was added from day 1. Error bars represent the mean ± SEM, n = 3. * P < 0.05; ** P < 0.01; *** P < 0.001; **** P < 0.0001.

(**f**) The expression of PRSS23 and cleaved PARP in the WCE from PRSS23-silenced GCSC1 cells and control cells. Expression was detected by western blot analysis. GAPDH was used as a loading control.

(**g**) The expression of PRSS23 and cleaved PARP in the WCE from GCSC-Vec and GCSC-PRSS23 cells was detected by western blot analysis. GAPDH was used as a loading control.

(**h**) The cell viability after treatment with or without tipranavir in control GC (AGS and HGC-27) cells (siNC) and PRSS23-silenced GC cells (siPRSS23-1/ siPRSS23-2). Cell viability was measured using a CCK-8 assay at the indicated times. Tipranavir was added from day 1. Error bars represent the mean ± SEM, n = 3. **** P < 0.0001.

(**i**) The expression of PRSS23 and cleaved PARP in the WCE from PRSS23-silenced GC cells and control cells. Expression was detected by western blot analysis. GAPDH was used as a loading control.

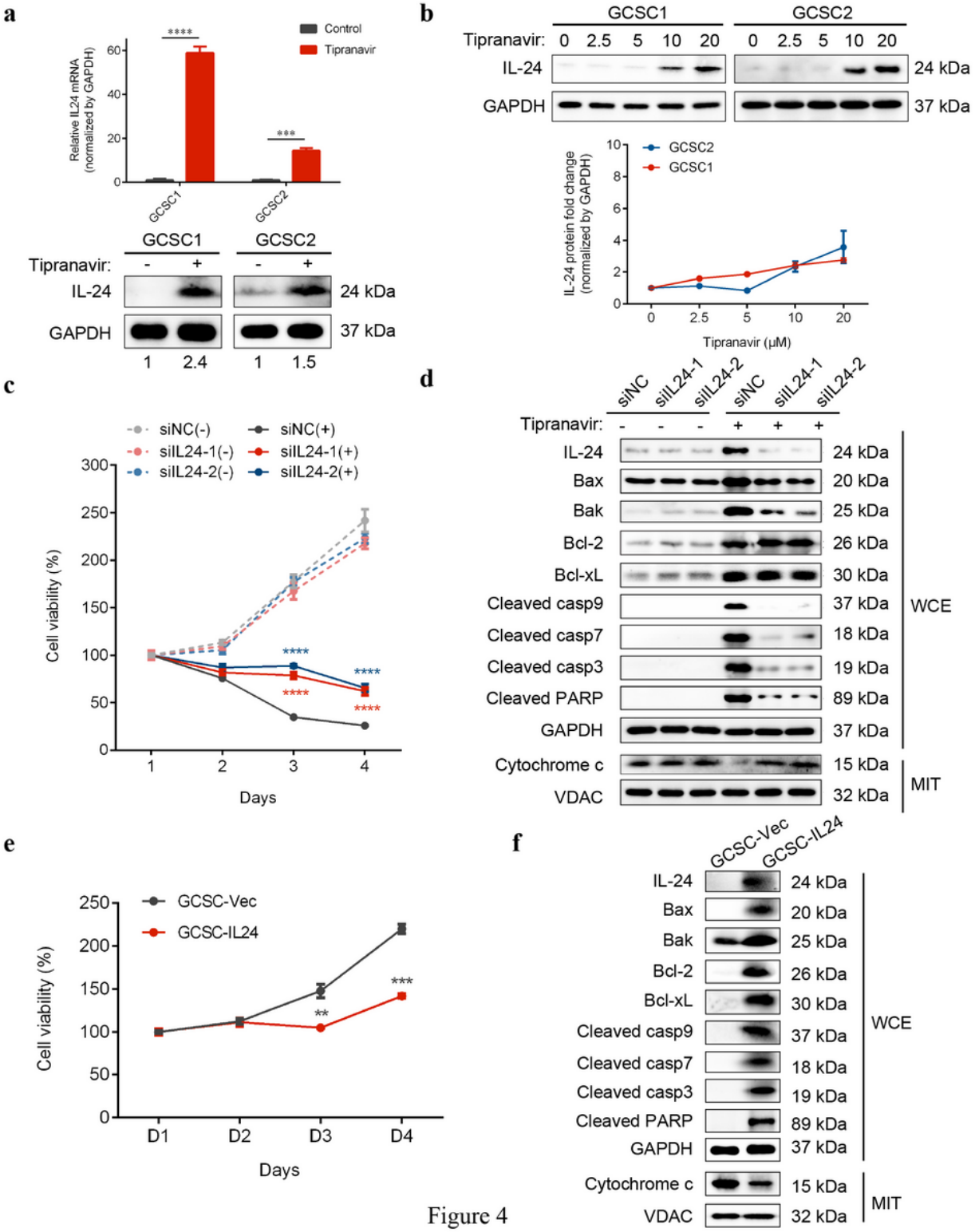

Figure 4

Figure 4

Tipranavir promotes GCSC apoptosis by inducing IL24 expression.

(**a**) Relative mRNA levels of IL24 in GCSC1 and GCSC2 cells treated with or without tipranavir for 24 hr. GAPDH was used as an internal control. Error bars represent the mean ± SEM, n = 3. *** P < 0.001; **** P < 0.0001.

(**b**) The expression of IL24 in GCSC1 and GCSC2 with or without tipranavir treatment for 48 hr. Expression was detected by western blot analysis, and quantitative data of the relative protein expression is illustrated. GAPDH was used as a loading control.

(**c**) The expression of IL24 in GCSC1 and GCSC2 cells treated with the indicated concentrations of tipranavir for 48 hr. Expression was detected by western blot analysis. GAPDH was used as a loading control.

(**d**) Quantitative data of the relative protein expression of IL24 from GCSC1 and GCSC2 shown in panel (c). Error bars represent the mean ± SEM, n = 3.

(**e**) Cell viability after treatment with or without tipranavir in control GCSC1 cells (siNC) and IL24-silenced GCSC1 cells (siIL24-1/siIL24-2). Cell viability was measured using a CCK-8 assay at the indicated times. Tipranavir was added from day 1. Error bars represent the mean ± SEM, n = 3. **** $P < 0.0001$.

(**f**) The expression of IL24, Bax, Bak, Bcl-2, Bcl-xL, cleaved caspase-9, cleaved caspase-7, cleaved caspase-3 and cleaved PARP in the WCE, and cytochrome c in the mitochondria from IL24-silenced GCSC1 cells and control cells with or without tipranavir treatment for 48 hr. Expression was detected by western blot analysis. GAPDH or VDAC was used as a loading control.

(**g**) The viability of GCSC2 cells (GCSC-Vec) and IL24-overexpressing GCSC2 cells (GCSC-IL24). Cell viability was measured using a CCK-8 assay at the indicated times. Tipranavir was added from day 1. Error bars represent the mean ± SEM, n = 3. ** $P < 0.01$; *** $P < 0.001$.

(**h**) The expression of IL24, Bax, Bak, Bcl-2, Bcl-xL, cleaved caspase-9, cleaved caspase-7, cleaved caspase-3 and cleaved PARP in the WCE, and cytochrome c in the mitochondria from GCSC-Vec and GCSC-IL24 cells, Expression was detected by western blot analysis. GAPDH or VDAC was used as a loading control.

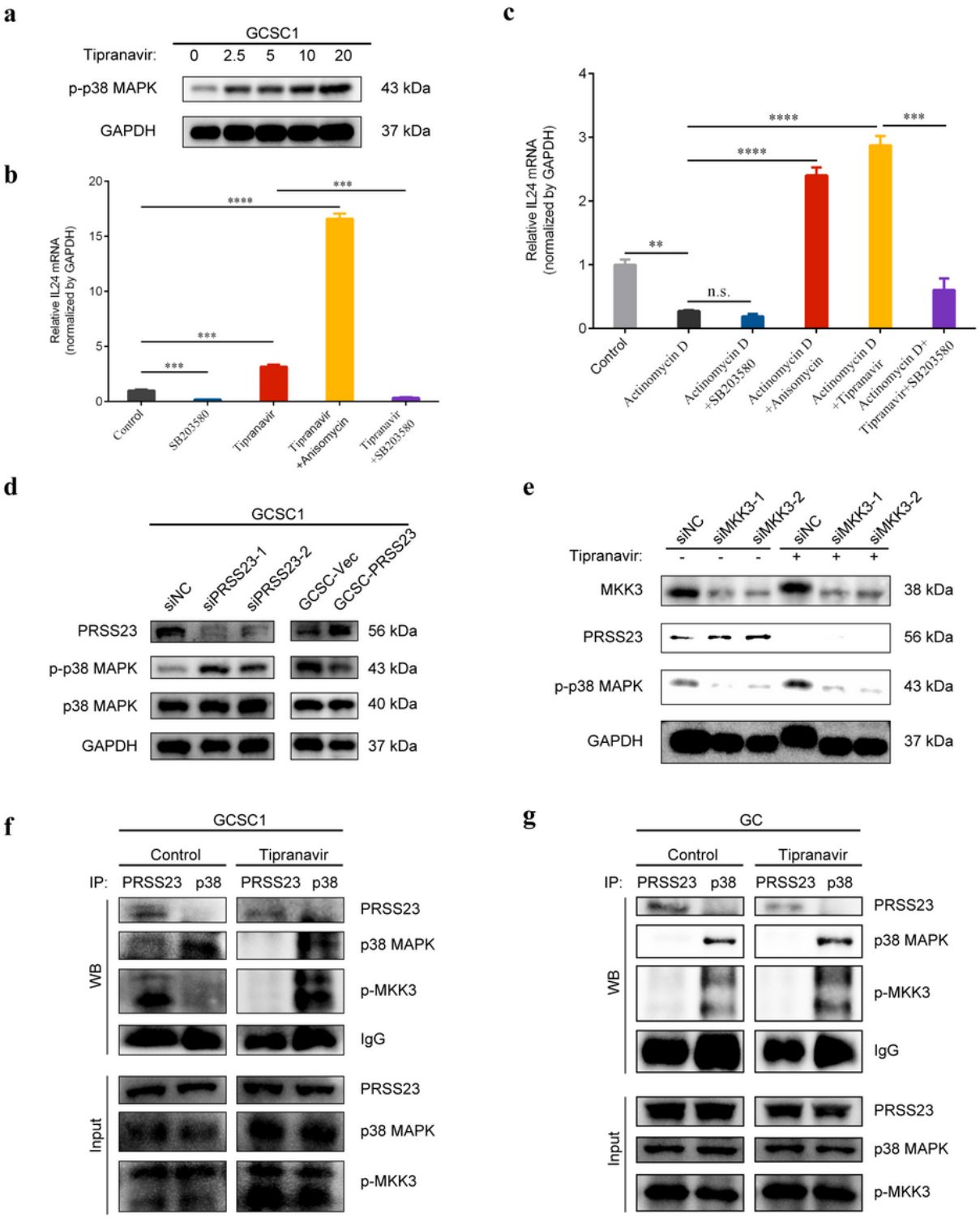

Figure 5

Figure 5

The PRSS23/MKK3/p38 MAPK pathway activates the IL24-dependent mitochondrial apoptotic pathway in GCSCs.

(**a**) The expression of phosphorylated p38 MAPK (p-p38 MAPK) and total p38 MAPK (p38 MAPK) in GCSC1 cells treated with the indicated concentrations of tipranavir for 48 hr. Expression was detected by

western blot analysis. GAPDH was used as a loading control.

(**b**) The relative mRNA levels of IL24 in GCSC1 cells treated with or without SB203580 (10 μM), anisomycin (5 μM), or tipranavir (20 μM) for 3 hr. GAPDH was used as an internal control. Error bars represent the mean ± SEM, n = 3. * P < 0.05.

(**c**) The expression of IL24 in GCSC1 cells pre-incubated with actinomycin D (10 μg/ml) for 1 hr before treatment with medium or SB203580 (10 μM), tipranavir (20 μM) for 2 hr. GAPDH was used as an internal control. Error bars represent the mean ± SEM, n = 3. * P < 0.05.

(**d**) The expression of PRSS23, phosphorylated p38 MAPK (p-p38 MAPK), total p38 MAPK (p38 MAPK) in the WCE from PRSS23-silenced GCSC1 cells, or GCSC2 cells (GCSC-Vec) and PRSS23-overexpressing GCSC2 cells (GCSC-PRSS23), and control cells. Expression was detected by western blot analysis. GAPDH was used as a loading control.

(**e**) The expression of MKK3, PRSS23, phosphorylated p38 MAPK (p-p38 MAPK) in the WCE from MKK3-silenced GCSC1 cells and control cells with or without tipranavir treatment for 48 hr. Expression was detected by western blot analysis. GAPDH was used as a loading control.

(**f**) Binding of phophorylated MKK3 (p-MKK3) to PRSS23, or phophorylated MKK3 (p-MKK3) to p38 MAPK from GCSC1 cells treated with or without tipranavir for 48 hr. Immunoprecipitation was used to detect protein binding. Proteins from whole lysates were used as a loading control.

(**g**) Binding of phosphorylated MKK3 (p-MKK3) to p38 MAPK from GC cell line (HGC-27) cells treated with or without tipranavir for 48 hr. Immunoprecipitation was used to detect protein binding. Proteins from whole lysates were used as a loading control.

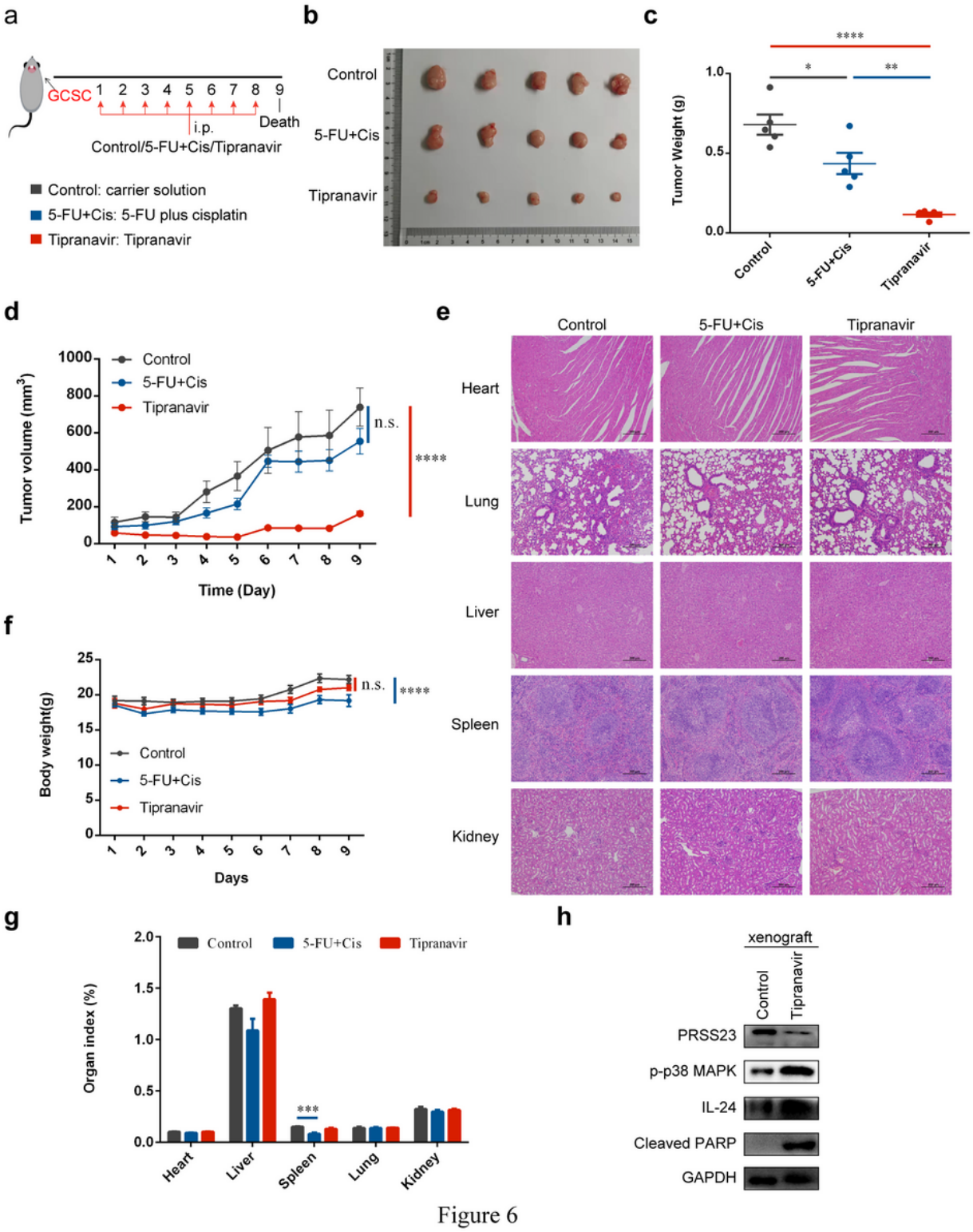

Figure 6

Figure 6

Tipranavir inhibits GCSC-derived tumor growth without apparent toxicity.

(**a**) A schematic showing the treatment regimen for tipranavir or 5-FU+Cis in nude mice with GCSCs-derived xenografts. BALB/c nude mice with GCSCs-derived xenograft tumors of 5 mm in diameter were randomly separated into three groups and treated with either tipranavir (25 mg/kg/mouse), 5-FU plus

cisplatin (5-FU: 20 mg/kg/mouse; cisplatin: 2 mg/kg/mouse) or carrier solution every day for 8 days. Drugs were administered as intraperitoneal injections.

(**b**) Images of xenografts at the end of the experiment from the tipranavir-treated, 5-FU+Cis-treated and control groups (five animals for each group).

(**c**) Tumor weights of end-point xenografts from tipranavir-treated, 5-FU+Cis-treated, and control (as indicated) groups of mice. Error bars represent the mean ± SEM, n = 5. Statistics: Student's t-test. *P < 0.05; ** P < 0.01; **** P < 0.0001.

(**d**) The tumor volume of tipranavir-treated, 5-FU+Cis-treated and control (as indicated) groups of mice. The tumor volume was measured at the indicated times. Error bars represent the mean ± SEM, n = 5. Statistics: two-way ANOVA. **** P < 0.0001; n.s., P > 0.05.

(**e**) Representative H&E staining images of major organs (heart, lung, liver, spleen, kidney) of tipranavir-treated, 5-FU+Cis-treated, and control (as indicated) groups of mice. Scale bar, 200 μm.

(**f**) The body weight of tipranavir-treated, 5-FU+Cis-treated, and control (as indicated) groups of mice. Error bars represent the mean ± SEM, n = 5. Statistics: two-way ANOVA. **** P < 0.0001; n.s., P > 0.05.

(**g**) The organ coefficients of tipranavir-treated, 5-FU+Cis-treated, and control (as indicated) groups of mice. Organ coefficients were measured at the end of the experiment. Error bars represent the mean ± SEM, n = 4. Statistics: Student's t-test. *** P < 0.001.

(**h**) The expression of PRSS23, phosphorylated p38 MAPK (p-p38 MAPK), IL24, cleaved PARP in tumor tissues from tipranavir-treated and control mice. Expression was detected by western blot analysis. GAPDH was used as a loading control.

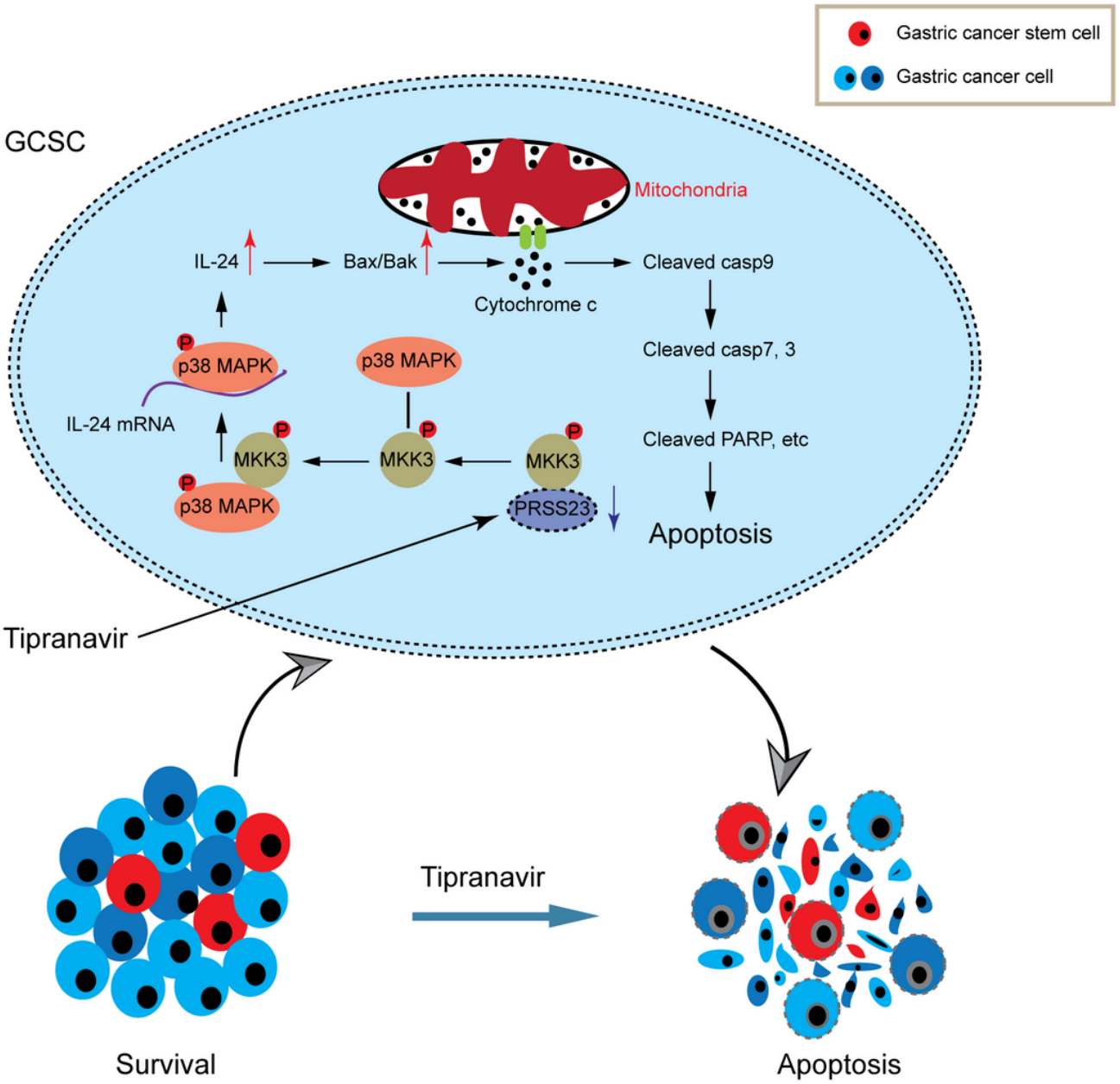

Figure 7

Figure 7

The proposed mechanism by which tipranavir induced GCSC apoptosis. Tipranavir decreases the expression of PRSS23, releasing phosphorylated MKK3 from the PRSS23/phospho-MKK3 complex to activate p38 MAPK, thus activating the IL24-mediated Bax/Bak mitochondrial apoptotic pathway.

Supplementary Files

This is a list of supplementary files associated with this preprint. Click to download.

- SupplementaryInformation.pdf